The vacuum UV photoabsorption spectrum of the geminal dichloroethylene (1,1-$C_2H_2Cl_2$) in the 5–20 eV range. A vibrational analysis of the valence and Rydberg states

To cite this article: R Locht *et al* 2017 *J. Phys. Commun.* **1** 045013

Journal of Physics Communications

PAPER

The vacuum UV photoabsorption spectrum of the geminal dichloroethylene (1,1-$C_2H_2Cl_2$) in the 5–20 eV range. A vibrational analysis of the valence and Rydberg states

R Locht[1], D Dehareng[2] and B Leyh[1]

[1] Molecular Dynamics Laboratory, Department of Chemistry, Building B6c, University of Liège, Sart-Tilman, B-4000 Liège 1, Belgium
[2] Center for Protein Engineering, Department of Life Sciences, Building B6a, University of Liège, Sart-Tilman, B-4000 Liège 1, Belgium

E-mail: robert.locht@ulg.ac.be

OPEN ACCESS

RECEIVED
14 June 2017

REVISED
5 October 2017

ACCEPTED FOR PUBLICATION
16 October 2017

PUBLISHED
14 November 2017

Keywords: vacuum UV photoabsorption spectroscopy, synchrotron radiation, 1,1-$C_2H_2Cl_2$, valence transitions, Rydberg transitions, vibrational structure, quantum chemical calculations

Abstract

The vacuum UV photoabsorption spectrum of 1,1-$C_2H_2Cl_2$ is presented and discussed in detail in the 6–20 eV photon energy range. The broad band observed at 6.488 eV includes the $2b_1(\pi) \rightarrow \sigma^*$, $2b_1(\pi) \rightarrow \pi^*$ valence transitions and the $2b_1(\pi) \rightarrow 3s$ Rydberg transitions. A quantum chemical calculation analysis is proposed and applied to the intertwined vibrational structure belonging to these transitions. For the $\pi \rightarrow \sigma^*$ and $\pi \rightarrow \pi^*$ transitions short vibrational progressions are observed, analyzed and tentatively assigned. The $\pi \rightarrow 3s$ Rydberg transition is characterized by a single progression starting at 6.746 eV. The fine structure observed between 7.5 and 10.1 eV has been analyzed in terms of vibronic transitions to ns- ($\delta = 0.89$), np- ($\delta = 0.59$ and 0.37) and nd-type ($\delta = 0.16$) Rydberg states all converging to the 1,1-$C_2H_2Cl_2^+(\tilde{X}^2B_1)$ ionic ground state. The vibrational structure analysis excitation leads to the following wavenumbers: $\omega_2 \approx 1310$ cm^{-1} (162 meV), $\omega_4 \approx 650$ cm^{-1} (81 meV) and $\omega_5 \approx 290$ cm^{-1} (37 meV). These modes can be assigned to the C=C stretching, to the symmetric C–Cl stretching and to the symmetric Cl–C–Cl bending vibrations respectively. By the same way, eight other Rydberg states were analyzed. For the first time the vacuum UV spectrum of 1,1-$C_2H_2Cl_2$ has been recorded in the 10–20 eV range, revealing intense broad bands which are assigned to transitions to Rydberg states converging to excited states of 1,1-$C_2H_2Cl_2^+$. Assignments are also proposed for the vibrational excitations observed in this range.

1. Introduction

Further to their wide interest in many fields of both pure and applied chemistry, we initiated a few years ago the systematic investigation of ethylene and its halogenated derivatives. Several experimental methods are coupled to quantum chemical calculations. The results about the monosubstituted C_2H_3X (X = F, Cl and Br) have been reported [1]. The influence of the nature of the substituent on the properties of the neutral (valence and Rydberg) states and the cationic states were discussed in detail.

Following an early study of the three C_2H_2FCl isomers [2] by vacuum UV photoabsorption and photoelectron spectroscopy we reported a detailed investigation of the 1,1-$C_2H_2F_2$ molecular system by the same techniques [3]. With respect to C_2H_3F [1] and 1,1-C_2H_2FCl [2, 4] substitutional effects were observed on, e.g., the $\pi \rightarrow \pi^*$ transition whereas the 3s-Rydberg transition energy remains almost unaffected.

Unlike the situation for its two 1,2-isomers, the 1,1-$C_2H_2Cl_2$ vacuum UV photoabsorption spectroscopic data are very scarce in the literature. To our knowledge the earliest vacuum UV photoabsorption spectrum of the 1,1-$C_2H_2Cl_2$ molecule has been observed by Teegan and Walsh [5] in the 2100–1100 Å (5.9–11.3 eV) spectral region using a normal incidence vacuum spectrograph. A classification of the Rydberg transitions and ionization energies of the [C = C]-π and the Cl-lone pair orbitals were proposed.

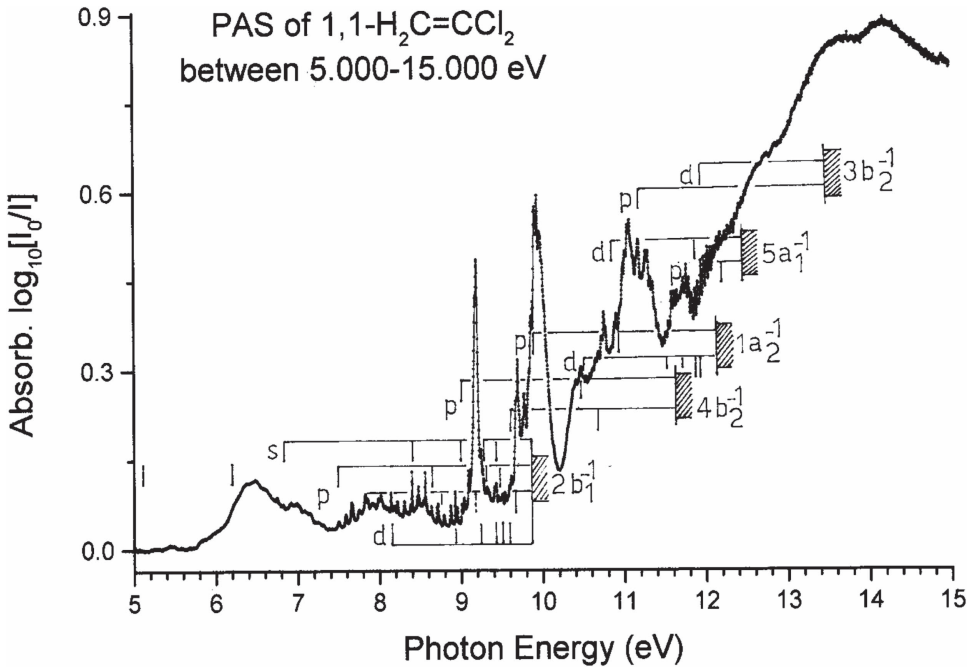

Figure 1. VUV photoabsorption spectrum of 1,1-$C_2H_2Cl_2$ between 5 eV and 15 eV. Rydberg states and their corresponding ionization continua are represented by vertical bars converging to shaded areas.

One of the latest vacuum UV photoabsorption spectra of the same molecule, in the same spectral region, has been reported by Walsh *et al* [6]. Besides a revision of the Rydberg series classification, a vibrational analysis and a corrected value of the lowest ionization energy have been presented. In a work on the photochemistry of chloroethylenes, Berry [7] measured the vacuum UV absorption spectrum of 1,1-$C_2H_2Cl_2$ between 260 and 140 nm (4.77–8.86 eV) but limited his analysis to the broad band between 240 and 180 nm (5.17–6.89 eV).

The present paper focuses on the vacuum UV photoabsorption spectrum of 1,1-$C_2H_2Cl_2$ (i) in the still unexplored range between 11.3 and 20 eV with medium resolution and (ii) in the 5.0–13.0 eV spectral region at higher resolution. The vibrational structure observed in the latter region will be analyzed.

2. Experimental

The experimental setup used in this work is the same as in previous works, using two VUV normal incidence monochromators from both BESSY synchrotron radiation facilities (Berlin, Germany) [1]. The first one, with a focal length of 1.5 m, allowed us to reach a resolving power of 1200 at 10 eV photon energy. It has been used in the 5–25 eV photon energy range. The accuracy of the energy scale calibration is estimated to be of the order of 2 meV and the peak position uncertainties are estimated to be ±4 meV. The second monochromator, used for high resolution measurements has a focal length of 3 m and leads to a resolving power of at least 13 000 at 10 eV. The peak position precision is ±2 meV. 1,1-$C_2H_2Cl_2$ from Aldrich (99% purity) was used without further purification.

To facilitate the characterization of weak signals superimposed on a continuum, we applied a FFT-based continuum subtraction procedure described previously [1, 3] and thoroughly investigated and validated by Marmet [8] and Carbonneau [9]. Recently, Palmer *et al* [10] applied a similar procedure to investigate the vacuum UV photoabsorption spectrum of the monohalobenzenes. The resulting continuum-free spectra are designated as Δ-plots.

3. Experimental results

The vacuum UV photoabsorption spectrum (PAS) of 1,1-$C_2H_2Cl_2$ between 5 and 15 eV photon energy is represented in figure 1 in terms of the absorbance $\log_{10}[I_0/I]$ as a function of the photon energy $h\nu$ (eV).

The PAS is made of three regions with very different characteristics: (i) in the 5.0–7.5 eV range a number of weak broad bands are superimposed on a weak continuum; (ii) the 7.5–13 eV region contains a large number of weak to very strong sharp structures and bands superimposed on a very weak continuum with increasing intensity from 9 eV upwards; (iii) above 13 eV and up to 20 eV several weak broad bands are superimposed on a

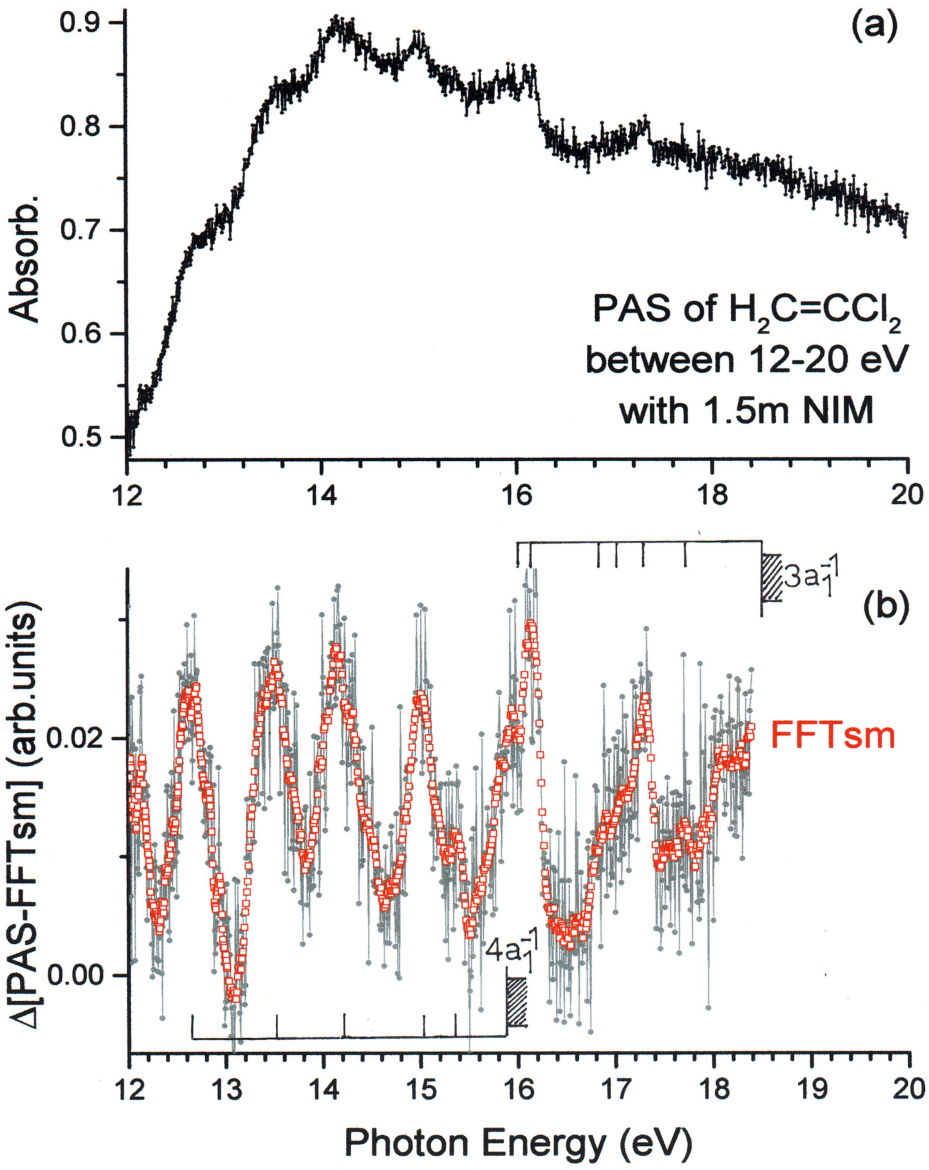

Figure 2. VUV photoabsorption spectrum of 1,1-$C_2H_2Cl_2$ between 12 and 20 eV photon energy: (a) direct absorbance spectrum as recorded with a 1.5 m NIM monochromator, (b) Δ-plot. The red curve (fast Fourier transformed = FFTsm) corresponds to the slight smoothing of the data in gray. Vertical bars indicate the band maxima and shaded area correspond to the ionization thresholds.

strong continuum as shown in figure 2(a). Therefore, the latter region is also displayed by a Δ-plot (figure 2(b)) in which the structures to be considered are enhanced.

In both figures vertical bars locate the structures and Rydberg series which will be considered in the following discussion. Shaded areas indicate the different convergence limits. The position in energy of the transitions to the vibrationless Rydberg states converging to the $\tilde{X}^2B_1$ ionic ground state and the successive ionic excited states are listed in tables 1 and 2 together with previously reported data [6].

4. *Ab initio* calculations

4.1. Methods

The Gaussian 09 set of programs [12] was used for all calculations with the aug-cc-pVDZ basis set, which includes polarization and diffuse basis functions [13]. For comparison purposes, additional calculations were performed without diffuse functions (cc-pVDZ).

Table 1. Rydberg series observed in the vacuum UV photoabsorption spectrum of 1,1-$C_2H_2Cl_2$ converging to the $\tilde{X}^2B_1$ (1,1-$C_2H_2Cl_2^+$) ionic ground state at $IE_{ad} = 9.826$ eV. The energy positions (eV), wavenumbers (cm^{-1}), effective quantum numbers (n^*), average quantum defects ($\bar{\delta}$) and assignments proposed in this work are provided. Comparison is made with the literature data [6]. Conversion factor: 1 eV = 8 065.545 eV [11].

This work			[6]
eV	cm^{-1}	n^*	(cm^{-1})
$2b_1 \rightarrow ns$ ($\bar{\delta} = 0.89 \pm 0.03$)			
6.746	54 410	2.102	
8.406	67 799	3.095	
9.016	72 719	4.098	
9.300	75 009	5.086	
9.464	76 332	6.130	
9.560	77 107	7.152	
$2b_1 \rightarrow np\sigma$ ($\bar{\delta} = 0.59 \pm 0.05$)			
7.508	60 556	2.533	
8.716	70 299	3.536	
9.128	73 622	4.480	
9.358	75 477	5.480	
9.488	76 526	6.460	
9.582	77 284	7.467	
9.638	77 735	8.646	
9.678	78 058	9.588	
9.704	78 268	10.560	
9.720	78 397	11.329	
9.742	78 574	(12.727)	
9.786	78 929	18.443	
$2b_1 \rightarrow np\pi$ ($\bar{\delta} = 0.37 \pm 0.05$)			
7.864	63 427	2.633	60 500
8.796	70 944	3.634	70 221
9.198	74 187	4.654	73 952
9.519	76 776	5.657	75 787
—	—	—	76 850
9.648	77 816	8.743	
9.678	78 058	9.588	
9.704	78 268	10.560	
9.720	78 397	11.329	
9.742	78 574	12.727	
9.764	78 752	14.814	
9.782	78 897	17.585	
9.786	78 929	18.443	
$2b_1 \rightarrow nd$ ($\bar{\delta} = 0.16 \pm 0.07$)			
8.150	65 734	2.849	65 657
8.936	72 074	3.910	72 001
9.244	74 558	4.835	74 791
9.426	76 026	5.832	76 260
9.544	76 978	6.946	
9.602	77 445	(7.793)	77 162
9.648	77 816	8.743	77 726
9.742	78 574	12.727	
9.764	78 752	14.814	

The vertical excitation energies for the low-lying excited states have been calculated at the ground state geometry optimized at the DFT-M06-2X level [14]. The geometries of the first three excited states have been optimized at the TDDFT [15] level.

Table 2. Rydberg series converging to the excited states of 1,1-$C_2H_2Cl_2^+$ observed. in the vacuum UV photoabsorption spectrum. The energy positions (eV), wavenumbers (cm^{-1}), effective quantum numbers (n^*) and assignments proposed in this work are provided. Conversion factor: 1 eV = 8 065.545 eV [11].

eV	cm^{-1}	n^*	Assign.
	$4b_2 \rightarrow np$[a]		
9.016	72 719	2.347	3pσ
10.482	84 543	3.417	4pσ
9.602	77 445	2.646	3pπ
10.694	86 253	3.688	4pπ
	$1a_2 \rightarrow np/nd$[b]		
9.904	79 881	2.46	3pπ
10.994	88 672	3.42	4pπ
10.552	85 108	2.91	3d
11.590	93 480	4.92	5d
11.732	94 625	5.97	6d
11.878	95 802	7.04	7d
11.948	96 367	8.99	9d
	$5a_1 \rightarrow np/nd$[b]		
12.056	97 238	5.612	6pπ
12.224	98 755	7.467	8pσ
10.812	87 205	2.89	3d
11.932	96 238	4.94	5d
	$3b_2 \rightarrow np/nd$[b]		
11.182	90 189	2.411	3pσ
11.996	96 754	2.986	3d
	$4a_1 \rightarrow ns/np/nd$[b]		
12.63	101 868	2.06	3s
13.54[c]	109 207	2.44	3p
14.15	114 127	2.85	4s/3d
14.27	115 095	2.96	3d
14.52	117 112	3.23	4s
15.00	120 983	4.07	5s/4d
15.20	122 596	4.68	5p
15.36	123 887	5.44	6p
	$3a_1 \rightarrow ns/np/nd$[b]		
15.94	128 565	2.31	3p
16.15[d]	130 178	2.40	
16.91[e]	136 388	2.92	4s/3d
17.08	137 760	3.09	
17.30[d]	139 534	3.37	4p
17.70	142 760	4.12	5s/4d

[a] For practical reasons (see text) the convergence limit considered in these transitions is the vertical ionization energy IE_{vert} = 11.647 eV.

[b] The convergence limits considered in these transitions are the adiabatic ionization energy values IE_{ad}.

[c] Nearly resonant with the ArII-resonance line at 13.48 eV [17].

[d] Absorption band with an asymmetric profile.

[e] Nearly resonant with the NeI-resonance lineat 16.85 eV [17].

Table 3. Optimized geometries of the ground and of the first three low-lying electronic excited states of neutral 1,1-$C_2H_2Cl_2$, determined in the C_2v symmetry point group. Internuclear distances in Å and angles in degree.

State	C–C	C–H	C–Cl	H–C–C	Cl–C–C
Ground state	1.3271	1.0866	1.7325	120.054	122.914
First excited	1.3944	1.0884	**1.9544**	119.920	**106.850**
Second excited	**1.4651**	1.0869	1.6796	119.167	119.267
Third excited	1.3981	1.0908	1.6914	119.190	120.720

Table 4. Vertical excitation energies (eV) to neutral states of 1,1-$C_2H_2Cl_2$ obtained at the TDDFT level. The calculations were performed with the aug-cc-pVDZ and cc-pVDZ (in parentheses) basis sets.

E_{vert}(eV)	E_{ad}(eV)	Description
1st exc. state 6.15[a] (6.44)	4.73	$\pi \rightarrow \sigma^*$, $\pi \rightarrow$ 3s
2nd exc. state 6.46 (7.01)	5.99	$\pi \rightarrow \pi^*$
3rd exc. state 6.66[a] (7.04)	6.46	$\pi \rightarrow$ 3s, +a small ($\pi \rightarrow \sigma^*$) contribution
6.7		$\pi \rightarrow$ 3d, $\pi \rightarrow$ 3p
7.26 (7.49)		n_σ(Cl) $\rightarrow \pi^*$
7.39 (7.68)		n_σ(Cl) $\rightarrow \sigma^*$
7.48		$\pi \rightarrow$ 3p
7.57		$\pi \rightarrow$ 3p
7.85 (8.04)		n_σ(Cl) $\rightarrow \pi^*$
7.95 (8.25)		n_σ(Cl) $\rightarrow$ 3p, n_σ(Cl) $\rightarrow$ 4d
7.98 (8.28)		$n\pi$(Cl) $\rightarrow$ 3p, $n\pi$(Cl) $\rightarrow$ 4d
8.01 (8.31)		$n\pi$(Cl) $\rightarrow \pi^*$

[a] The MO involved in this excitation has an important Cl-lone pair character.

4.2. Presentation of the results

The optimized geometry parameters are presented in table 3.

The vertical excitation energies of several states are presented in table 4, as well as the adiabatic excitation energies for the first three states.

The cc-pVDZ basis set was used for comparison purposes to emphasize the valence character of the excitations, since it does not include diffuse functions. Our results show that four states are superimposed around 6–7 eV. It also appears from these calculations that the first state shows a mixed $\pi \rightarrow \sigma^*$ and $\pi \rightarrow$ 3s character, and in a much less pronounced way, the third state also presents a major $\pi \rightarrow$ 3s and a minor $\pi \rightarrow \sigma^*$ mixed character. Such Rydberg–valence interactions involving σ^* antibonding orbitals and the associated 'Rydbergisation' phenomenon have been reviewed by Ashfold *et al* [16].

The optimized geometry of the first excited valence state is characterized by a very large C–Cl bond length, related to the antibonding character of the σ^* MO populated by the excitation. Due to the large equilibrium internuclear distance, this state is most probably nearly repulsive (low dissociation energy), so that its excitation is expected to produce a broad continuous band.

5. Discussion

The molecular orbital configuration of 1,1-$C_2H_2Cl_2$ in the C_{2v} symmetry group is described by

$$1s^2(Cl1)\ 1s^2(Cl2)\ 1s^2(C1)\ 1s^2(C2)\ 2s^2(Cl1)\ 2s^2(Cl2)\ 2p^6(Cl1)\ 2p^6(Cl2)$$
$$1a_1{}^2 1b_2{}^2 2a_1{}^2 3a_1{}^2 2b_2{}^2 4a_1{}^2 1b_1{}^2 3b_2{}^2 5a_1{}^2 1a_2{}^2 4b_2{}^2 2b_1{}^2 :\ \tilde{X}^1A_1,$$

where $1a_1$ is the first outer-valence shell orbital.

We recently measured the HeI-photoelectron spectrum (PES) and the threshold photoelectron spectrum (TPES) of 1,1-$C_2H_2Cl_2$ and the results will be reported in a forthcoming paper [17]. The first adiabatic ionization energy is located at $IE_{ad}(1,1\text{-}C_2H_2Cl_2^+, \tilde{X}\ ^2B_1) = 9.826 \pm 0.002$ eV and the corresponding vertical value is $IE_{vert}(1,1\text{-}C_2H_2Cl_2^+, \tilde{X}^2B_1) = 9.993 \pm 0.004$ eV, in very good agreement with available data [18–21].

At higher energies eight bands were observed by HeI-PES. For most of them the adiabatic ionization energy (IE_{ad}) could be measured at 11.520, 12.157, 12.497, 13.521, 15.539 and 18.496 eV [17]. The PES-band shape corresponding to the first excited state has a symmetric bell-shaped envelope and its maximum is measured at $IE_{vert} = 11.647$ eV. The fifth and sixth PES-bands at 13.521 and 15.539 eV involve two overlapping electronic states [17]. For the two components vertical ionization energies (IE_{vert}) were measured at 13.633 and 14.195 eV for the former and at about 15.82 and 16.16 eV for the latter [17].

5.1. The valence transitions (see figures 1, 3(a) and 4).

The characteristic broad band observed at low energy in the vacuum UV PAS of the ethylenic compounds has its maximum at 6.488 eV in 1,1-$C_2H_2Cl_2$ (figure 1). Compared to our observations in ethylene and its halogenated derivatives investigated up to now [1–4], it is fairly weak and extends between 5.0 and 7.4 eV. To enhance the very weak structures superimposed on the continuum the subtraction method has been applied. Figure 3(a) shows the result on an expanded photon energy scale where the red curve in the upper part of the figure represents the continuum to be subtracted from the original signal. The result of this operation (Δ-plot) is displayed in the lower part of figure 3(a) which clearly shows three different parts: (a) a noisy weak series of three broad doublet structures, (b) a series of four narrower simple peaks and (c) the beginning of a series of very narrow peaks extending above 7.0 eV photon energy.

The very weak signal between 5.0 and 6.0 eV might be considered as the possible end of a longer vibrational progression belonging to a valence excited singlet state. Possibly the σ^*/3s state could be involved. Robin [22] mentioned a $\pi \rightarrow \sigma^*$ transition at 6.01 eV in the trans-1,2-$C_2H_2Cl_2$ isomer. By quantum mechanical calculations, Arulmozhiraja *et al* [23] calculated this transition energy at 6.25 eV. The broadness of the observed features, compared to higher-energy peaks may be linked to the short lifetime of these vibronic states which likely predissociate. Our quantum chemical calculations reveal important C–Cl bond lengthening at the optimized geometry of this state which could be nearly repulsive (see table 3). Several photodissociation studies have been reported in the wavelength region of 155–250 nm (8.00–4.96 eV) [7] or 222–304 nm (5.58–4.08 eV) [24] or at 214.5 nm (5.78 eV) and at 235 nm (5.28 eV) [25]. The loss of HCl [7] and $Cl(^2P_J)$ [24, 25] were investigated. Curve crossings between (π, π^*), (π, σ^*) and/or (n, σ^*) states were suggested. The observed structures in the 5.0–5.6 eV range may be associated with vibronic states which cannot be described by a first-order description separating the electronic and vibrational contributions.

Recent theoretical DFT calculations at B3LYP/6-311-G(d, p) level, devoted to the chloroethylenes, are reported by Khvostenko [26]. They are focused on the prediction of the transition energies to valence singlet and triplet states. They do not, however, provide details shedding new light on the physical situation in this energy range.

The four following features between 6.2 and 6.6 eV have a more regular spacing of on average 134 ± 5 meV (1080 ± 40 cm^{-1}) with a regular intensity distribution, and are narrower than the lower lying structures but broader than the higher-energy ones. For these reasons it is believed that they correspond to another valence excited state, e.g. the (π, π^*) state. The feature at 6.488 eV corresponds to the maximum of the broad band. Walsh *et al* [6] observed the intensity maximum of a continuum at about 51 814 cm^{-1} (or 6.42 eV) (see table 5).

The (π, π^*) state likely overlaps the (π, σ^*/3s) state below 6.2 eV and the Rydberg (π, 3s/σ^*) state above 6.7 eV. As shown in table 5, over the narrow energy window of 6.22–6.62 eV the vibrational spacing regularly decreases from 139 to 128 meV likely suggesting a strong anharmonicity. This vibrational spacing could correspond to a strongly weakened C=C bond owing to the antibonding character of the π^* MO. The C=C stretching vibration is characterized by a wavenumber of 1627 cm^{-1} (202 meV) in the neutral ground state [27].

The main interest of a systematic study of the PAS of a series of halogenated ethylenes is to emphasize the effect of the substitution on the energy of the different valence and lowest Rydberg states. A comparison of the PAS between 5.5 and 8.2 eV is displayed in figure 4(a) for Cl-substituted only [1] and in figure 4(b) for mixed F- and Cl-substituted [1–4] ethylenes investigated in our laboratory.

Comparing the PAS of the three chlorinated compounds in the 5–8 eV photon energy range, the position of the maximum of the underlying continuum (denoted as π_V^* in figure 4(a)) could be a measure of the shift to lower energy of the $\pi \rightarrow \pi^*$ vertical excitation energy induced by chlorination, as already pointed out by Robin [22]. In the PAS of the F- and Cl-substituted ethylenes a similar shift is observed for the $\pi \rightarrow \sigma_v^*$ transition (see figure 4(b)). The effect on the $\pi \rightarrow$ 3s Rydberg transition is less obvious. The vertical and the adiabatic excitation energy being likely fairly close [1–3, 6], the adiabatic values will be compared. As shown in figure 4(a), with respect to C_2H_4, the shift to lower energies is important upon Cl substitution but is quite insensitive to the number of Cl atoms. This trend is confirmed for the tri- and the tetrachloroethylene [22].

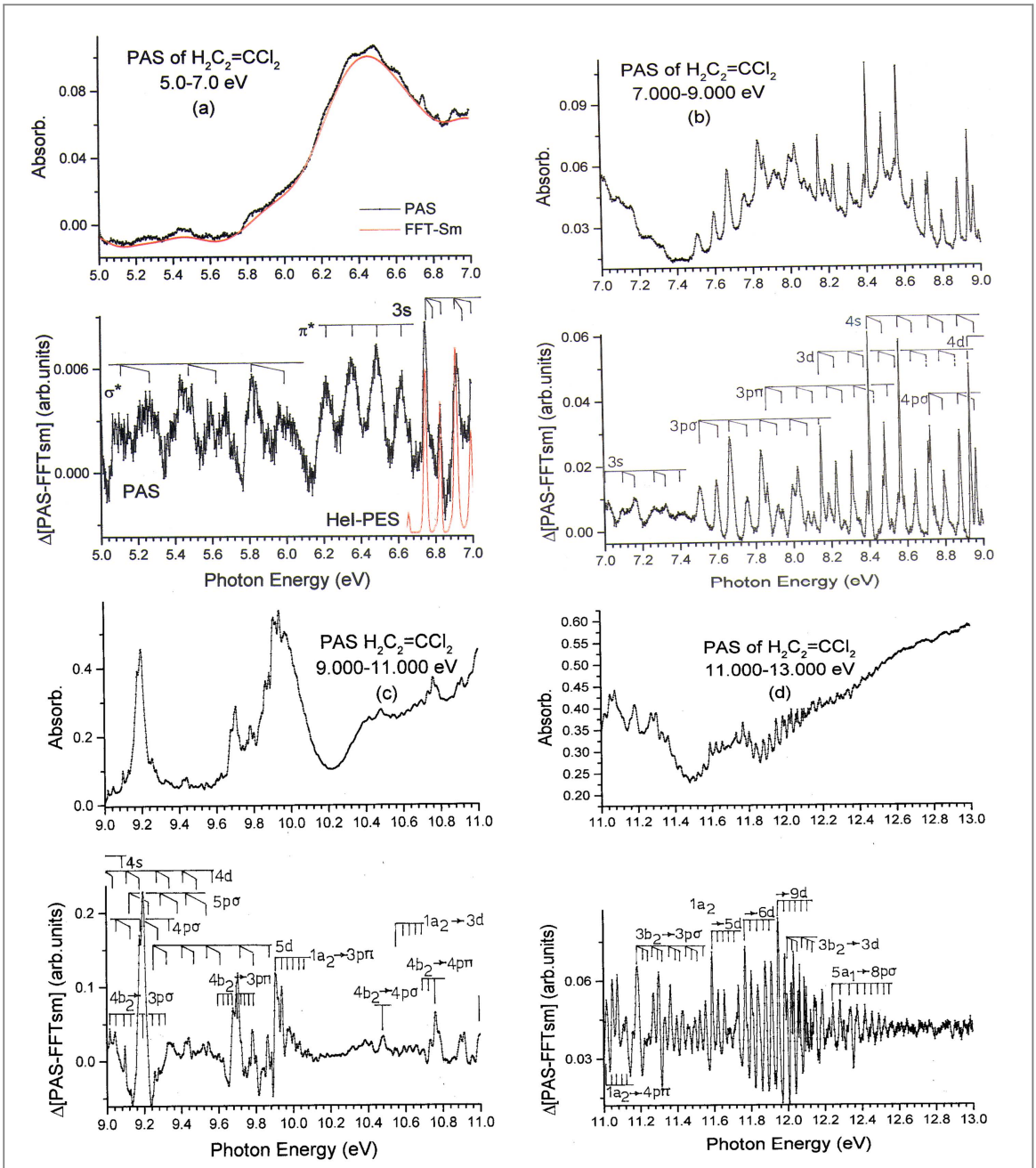

Figure 3. Expanded VUV photoabsorption spectrum of 1,1-$C_2H_2Cl_2$ between 5.0 and 13.0 eV. The upper and lower parts show the absorbance and the corresponding Δ-plot respectively for (a) 5.0–7.0 eV, (b) 7.0–9.0 eV, (c) 9.0–11.0 eV and (d) 11.0–13.0 eV. Long vertical bars indicate the vibrationless (0, 0) transitions to the indicated Rydberg transitions. For each transition, the progression(s) are identified by short vertical bars.

The substitution of an H atom in C_2H_4 by one or two F atoms induces a rather limited shift to higher energies on the $\pi \rightarrow \pi^*$ vertical transition energy, i.e., at 7.4 and 7.5 eV in C_2H_4 and 1,1,-$C_2H_2F_2$ [1, 3] (see figures 4(b)) and 7.6 eV in C_2H_3F [1]. Contrarily, the substitution of an H/F atom by a Cl atom provides a large shift to lower energies on the same transition: 7.4 eV in C_2H_4 to 6.9 eV in C_2H_3Cl [1], to 7.0 eV in 1,1-C_2H_2FCl [2, 4] and to 6.4 eV in 1,1-$C_2H_2Cl_2$.

5.2. The Rydberg transitions

As shown in figure 1, the PAS measured in the photon energy range of 7.4 eV to about 13.0 eV displays numerous structures of very variable intensities. Particularly from 7.4 eV up to about 10.0 eV the PAS exhibits long series of weak features besides two strong transitions. The wavy underlying continuum is fairly weak. This region is shown on an expanded energy scale between 7 and 13 eV in figures 3(b)–(d), the upper and lower part showing the original spectrum and the corresponding Δ-plot respectively.

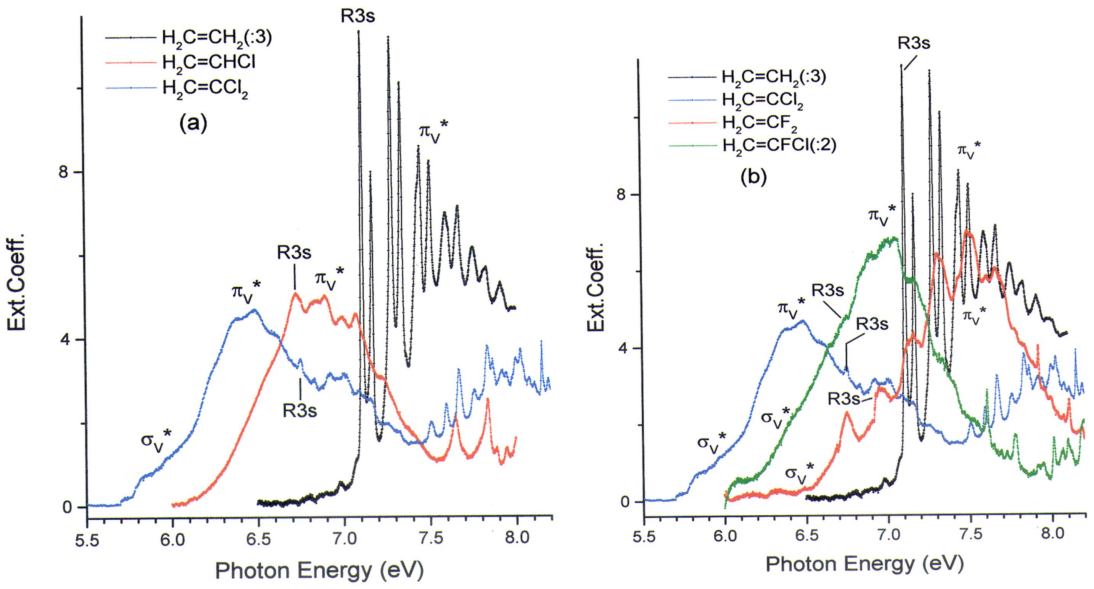

Figure 4. VUV photoabsorption spectra of (a) C_2H_4, C_2H_3Cl and 1,1-$C_2H_2Cl_2$ and (b) of C_2H_4, 1,1-$C_2H_2F_2$, 1,1-$C_2H_2Cl_2$ and 1,1-C_2H_2FCl on an expanded photon energy scale between 5.5 and 8.2 eV. The vertical excitation energies (index v) to the valence states (σ^* and π^*) and the adiabatic excitation energies to the Rydberg (3s) states are indicated for each molecule.

Table 5. Energy positions (eV), wavenumbers (cm^{-1}) and assignments proposed for the vibrational structures observed in the vacuum UV photoabsorption spectrum of 1,1-$C_2H_2Cl_2$ between 5.0 and 7.0 eV. Comparison is made with the literature data [6]. Conversion factor 1 eV = 8 065.545 cm^{-1} [11].

This work			[6]	
Energy (eV)	Wavenbr. (cm^{-1})	Assignments	Energy (cm^{-1})	Assignments
5.112	41 231	$(\sigma^*)\mathbf{v_1}$		
5.252	42 360	$(v_2 = 1)$		
5.460	44 038	$(v_1 + 1)$		
5.625	45 369	$(v_2 = 1)$		
5.815	46 901	$(v_1 + 2)$		
5.987	48 288	$(v_2 = 1)$		
6.215	50 127	$(\pi^*)\mathbf{v}$	51 814 (~193 nm)	Maximum intensity of the continuum
6.354	51 248	$(v + 1)$		
6.488	52 329	$(v + 2)$		
6.616	53 362	$(v + 3)$		
6.746	54 410	**R3s(0, 0)**		
6.781	54 692	ν_5		
6.827	55 063	ν_4		
6.892	55 588	$2\nu_4$		
6.913	55 757	$\boldsymbol{\nu_2}$		
6.943	55 999	$\nu_2 + \nu_5$		
6.989	56 370	na		
7.001	56 467	$\nu_2 + \nu_4$		
7.085	56 644	$\mathbf{2\nu_2}$		
7.113	57 370	$2\nu_2 + \nu_5$		
7.159	57 741	$2\nu_2 + \nu_4$		
7.189	57 983	$2\nu_2 + 2\nu_5$		
7.233	58 338	$2\nu_2 + 2\nu_4$		
7.245	58 435	$\mathbf{3\nu_2}$		
7.275	58 677	$3\nu_2 + \nu_5$		
7.307	58 935	$3\nu_2 + 2\nu_5$		
7.319	59 032	$3\nu_2 + \nu_4$		
7.408	59 749	$\mathbf{4\nu_2}$		

Due to the large number of Rydberg transitions accompanied by vibrational excitation, the assignment is attempted based on the Rydberg formula, even though this neglects the perturbations between Rydberg series. The previously mentioned relevant ionization thresholds are inserted in figure 1. The fine structure will be assigned mostly to the vibrational excitation involved in successive Rydberg transitions, rather than to Rydberg states with high principal quantum number n. The intensity distribution follows the Franck–Condon distribution in the former case, whereas in the latter case the intensity scales as $(n^*)^{-3} = (n - \delta)^{-3}$ where n^* is the effective quantum number and δ is the quantum defect, which is characteristic of a given Rydberg series. Robin [22] made a critical review of the analyses of Rydberg transitions and proposed rules and guidelines for assignments.

5.2.1. Rydberg transitions between 6.6 and 9.9 eV (see figure 1).

The vibrationless Rydberg transitions observed for 1,1-$C_2H_2Cl_2$ between 6.7 and 9.9 eV are shown in figure 1. All detected Rydberg transitions are reported in table 1 with their effective quantum numbers. In the same table the previous data set of Walsh *et al* [6] is included for comparison. As mentioned earlier (see section 2) the estimated uncertainty on the measurements in the present spectrum is about 2 meV or 16 cm^{-1}. No uncertainty estimation is provided by Walsh *et al* [6]. For the assignments reported in the present work the adiabatic ionization energy value $IE_{ad}(1,1\text{-}C_2H_2Cl_2^+, \tilde{X}^2B_1) = 9.826 \pm 0.002$ eV [17] has been used whereas the value determined by Walsh *et al* [6] was 9.85 eV.

Table 1 displays the excitation energies corresponding to the $\pi \rightarrow$ ns Rydberg series converging to the first ionization energy limit. It is observed up to $n = 8$ with an average quantum defect $\overline{\delta} = 0.89 \pm 0.03$. This series is not listed in the work of Walsh *et al* [6]. Only one Rydberg state vibrational progression starting at 67 730 cm^{-1} is mentioned [6], corresponding fairly well to 67 799 cm^{-1} (8.406 eV) in the present work and assigned to the vibrationless $\pi \rightarrow$ 4s Rydberg transition.

Two distinct $\pi \rightarrow$ npλ Rydberg series are observed (see table 1), like in C_2H_3Br [1], 1,1-C_2H_2FCl [2], 1,1-$C_2H_2F_2$ [3] and in the methyl monohalides CH_3X (X = Cl, Br and I) [28]. These series are assigned taking into account the quantum defect value. As the core contains less orbitals of π symmetry than of σ symmetry, the σ-type Rydberg orbitals are expected to interact more strongly with the ionic core and would therefore be characterized by a larger quantum defect.

The $\pi \rightarrow$ npσ Rydberg series is starting at 7.508 eV whereas its $\pi \rightarrow$ npπ counterpart starts at 7.864 eV. The splitting of 0.356 eV between the two npλ-type series is about twice as large as in 1,1-$C_2H_2F_2$ [3] where an energy difference of 0.183 eV is measured. In 1,1-C_2H_2FCl the corresponding splitting is 0.405 eV [2, 4]. The two series are observed up to high values of the principal quantum number. The average quantum defects $\overline{\delta} = 0.59 \pm 0.05$ and 0.37 ± 0.05 are determined for the npσ- and the npπ-type Rydberg series respectively.

A $\pi \rightarrow$ ndλ series starts at 8.150 and most of its members are characterized by an average quantum defect $\overline{\delta} = 0.16 \pm 0.07$. Only two members would be characterized by $\delta < 0.1$ likely suggesting the existence of a ndλ' series. In the vacuum UV spectrum of 1,1-$C_2H_2F_2$ [3] and of 1,1-C_2H_2FCl [2, 4] a ndσ series is observed with $\overline{\delta} = 0.14 \pm 0.02$ and $\overline{\delta} = 0.13 \pm 0.03$ respectively. For the corresponding ndπ series we inferred $\overline{\delta} = 0.04 \pm 0.03$ [3] and $\overline{\delta} = -0.11 \pm 0.02$ [2] respectively.

5.2.2. Vibrational analysis (see figures 3(a)–(c))

Let us consider the intense transitions between 6.6 and 13.0 eV. The intensity of the transitions to high n Rydberg states decreases rapidly, according to the $(n^*)^{-3}$ intensity scaling law. On the contrary, the intensity distribution of the vibrational transitions does not follow this law and can, therefore, become dominant.

To disentangle this spectrum, we assumed [22] that the vibrational wavenumbers of the Rydberg states within a series are similar to those of the ionic state to which this series converges. This approach has been shown efficient to interpret the vacuum UV spectra of the methyl halides [28], of C_2H_3F [1], and 1,1-$C_2H_2F_2$ [3]. The convergence limit of most of the Rydberg states involved between 6.7 and 9.9 eV is $IE_{ad}(1,1\text{-}C_2H_2Cl_2^+, \tilde{X}^2B_1) = 9.826 \pm 0.002$ eV [17]. The cationic $\tilde{X}^2B_1$ vibrational structure is dominated by the excitation of two vibrational normal modes characterized by the wavenumbers $\omega_3^+ = 1322 \pm 48$ cm^{-1} (0.163 ± 0.006 eV) and $\omega_4^+ = 653 \pm 24$ cm^{-1} (0.081 ± 0.003 eV) [17] (notation ω_i for the neutrals and ω_i^+ for the ions). Two other very weak vibrations were also observed [17]. However, more than 95% of the available intensity is distributed over the C=C stretching ν_3^+ and the C–Cl symmetric stretching ν_4^+. For the purpose of the decomposition of the PAS we used the corresponding HeI-PES as a reference which was shifted to make its vibrationless transition to coincide with that of the successive transitions to the Rydberg states (see figure 3(a), red curve, for an example).

The result of this procedure is represented in figures 3(a)–(c) and the energy positions and assignments are summarized in table 5 for the 3s Rydberg state and in table 6 for the remaining Rydberg state.

In the $\pi \rightarrow$ 3s transition region no comparison could be made with the results reported by Walsh *et al* [6]: only a continuum with an intensity maximum at 51 814 cm^{-1} (6.424 eV) has been mentioned.

Table 6. Energies (eV), wavenumbers (cm^{-1}) and assignments for the peaks in the photoabsorption spectrum of 1,1-$C_2H_2Cl_2$ between 7 and 10 eV (Rydberg series converging to the $\tilde{X}^2B_1$ ionic ground state). Comparison is made with the literature [6]. Conversion factor 1 eV = 8 065.545 eV [11].

This work			[6]	
Energy (eV)	Wavenbr. (cm^{-1})	Assignments	Wavenbr. (cm^{-1})	Assignments
		$2b_1 \rightarrow 3p\sigma, n^* = 2.423$		
7.508	60 556	**(0, 0)**	[60 500]	3p
7.538	60 798	ν_5		
7.596	61 266	ν_4	[61 209]	
7.648	61 685	$(4\nu_5)$		
7.668	61 846	**ν_3**	61 815	
7.756	62 556	$\nu_3 + \nu_4$	62 493	
7.786	62 798	$(\nu_3 + 3\nu_5)$		
7.808	62 976	$\nu_3 + 4\nu_5$		
7.832	63 169	**$2\nu_3$**	63 140	
7.918	63 863	$2\nu_3 + \nu_4$	63 783	
7.996	64 492	**$3\nu_3$**	[64 426]	
8.078	65 153	$3\nu_3 + \nu_4$	65 076	
		$2b_1 \rightarrow 3p\pi, n^* = 2.633$		
7.864	63 427	**(0, 0)**	63 349	
7.940	64 040	ν_4	64 047	
7.984	64 395	$(3\nu_5)$	[64 426]	
8.026	64 734	**ν_3**	64 671	
8.108	65 395	$\nu_3 + \nu_4$	65 328	
8.128	65 557	$\nu_3 + 3\nu_5$	[65 657]	
8.188	66 041	**$2\nu_3$**	65 969	
8.266	66 670	$2\nu_3 + \nu_4$		
8.346	67 315	**$3\nu_3$**		
8.446	68 121	$3\nu_3 + \nu_4$		
8.516	68 686	**$4\nu_3$**		
8.586	69 251	$4\nu_3 + \nu_4$		
8.614	69 477	$(4\nu_3 + 3\nu_5)$	69 575	

Table 6. (Continued.)

This work			[6]	
Energy (eV)	Wavenbr. (cm^{-1})	Assignments	Wavenbr. (cm^{-1})	Assignments
		$2b_1 \rightarrow 3d, n^* = 2.849$		
8.150	65 734	**(0, 0)**	[65 657]	
8.228	66 363	ν_4	66 302	
8.312	67 040	$\boldsymbol{\nu_3}$	66 973	
8.390	67 670	$\nu_3 + \nu_4$	67 610	
8.474	68 347	$\mathbf{2\nu_3}$	68 292	
8.554	68 993	$2\nu_3 + \nu_4$	68 925	
8.636	69 654	$\mathbf{3\nu_3}$	69 575	
[8.716]	70 299	$3\nu_3+\nu_4$	[70 310]	
8.788	70 880	$\mathbf{4\nu_3}$	70 888	
8.862	71 477	$4\nu_3 + \nu_4$	[71 551]	
		$2b_1 \rightarrow 4s, n^* = 3.095$		
8.406	67 799	**(0, 0)**	67 730	
8.486	68 444	ν_4	68 365	
8.567	69 098	$\boldsymbol{\nu_3}$	69 039	
8.646	69 735	$\nu_3 + \nu_4$	[69 668]	
8.726	70 380	$\mathbf{2\nu_3}$	[70 310]	
8.760	70 654	$2\nu_3 + \nu_5$		
8.808	71 046	$2\nu_3 + \nu_4$	[70 940]	
8.890	71 707	$\mathbf{3\nu_3}$		
8.981	72 441	$3\nu_3 + \nu_4$		
9.056	73 041	$\mathbf{4\nu_3}$		
		$2b_1 \rightarrow 4p\sigma, n^* = 3.499$		
[8.716]	70 299	**(0, 0)**	70 221	4p
8.796	70 944	ν_4	70 888	
8.880	71 622	$\boldsymbol{\nu_3}$	[71 551]	
8.965	72 308	$\nu_3 + \nu_4$	72 234	
9.044	72 945	$\mathbf{2\nu_3}$	72 879	

Table 6. (Continued.)

This work			[6]	
Energy (eV)	Wavenbr. (cm^{-1})	Assignments	Wavenbr. (cm^{-1})	Assignments
[9.128]	73 622	$2\nu_3 + \nu_4$	73 536	
[9.198]	74 187	$\mathbf{3\nu_3}$		
9.278	74 832	$3\nu_3 + \nu_4$		
9.358	75 477	$\mathbf{4\nu_3}$		
		$\mathbf{2b_1 \rightarrow 4d, n^* = 3.910}$		
8.936	72 074	**(0, 0)**	72 001	4d
9.016	72 719	ν_4	72 648	
9.098	73 380	$\mathbf{\nu_3}$	73 300	
9.178	74 026	$\nu_3 + \nu_4$	73 952	
9.258	74 671	$\mathbf{2\nu_3}$	74 620	
9.340	75 332	$2\nu_3 + \nu_4$	75 234	
9.426	76 026	$\mathbf{3\nu_3}$		
9.506	76 671	$3\nu_3 + \nu_4$		
9.582	77 284	$\mathbf{4\nu_3}$		
		$\mathbf{2b_1 \rightarrow 5p\sigma, n^* = 4.415}$		
[9.128]	73 622	**(0, 0)**		
[9.198]	74 187	ν_4		
9.300	75 009	$\mathbf{\nu_3}$		
9.368	75 558	$\nu_3 + \nu_4$		
9.464	76 332	$\mathbf{2\nu_3}$		
[9.544]	76 978	$2\nu_3 + \nu_4$		
		$\mathbf{2b_1 \rightarrow 5d, n^* = 4.835}$		
9.244	74 558	**(0, 0)**		
9.316	75 139	ν_4		
9.406	75 864	$\mathbf{\nu_3}$		
[9.488]	76 526	$\nu_3 + \nu_4$		
9.560	77 107	$\mathbf{2\nu_3}$		

Table 6. (Continued.)

This work			[6]	
Energy (eV)	Wavenbr. (cm^{-1})	Assignments	Wavenbr. (cm^{-1})	Assignments
9.638	77 735	$2\nu_3 + \nu_4$		
9.720	78 397	$\mathbf{3\nu_3}$		
9.800	79 042	$3\nu_3 + \nu_4$		
9.884	79 720	$\mathbf{4\nu_3}$		
		$\mathbf{2b_1 \rightarrow 6p\sigma, n^* = 5.391}$		
9.358	75 477	$\mathbf{(0,0)}$		
9.440	76 139	ν_4		
9.519	76 776	$\mathbf{\nu_3}$		
9.602	77 445	$\nu_3 + \nu_4$		
9.678	78 897	$\mathbf{2\nu_3}$		
9.764	78 752	$2\nu_3 + \nu_4$		
9.838	79 349	$\mathbf{3\nu_3}$		
9.920	80 010	$3\nu_3 + \nu_4$		
10.002	80 671	$\mathbf{4\nu_3}$		
		$\mathbf{2b_1 \rightarrow 7d, n^* = 6.946}$		
[9.544]	76 978	$\mathbf{(0,0)}$		
9.624	77 623	ν_4		
9.704	78 268	$\mathbf{\nu_3}$		
9.782	78 058	$\nu_3 + \nu_4$		
9.864	79 558	$\mathbf{2\nu_3}$		
9.938	80 155	$2\nu_3 + \nu_4$		
10.036	80 946	$\mathbf{3\nu_3}$		
10.120	81 623	$3\nu_3 + \nu_4$		

[a] Energy positions corresponding to two or more assignments are given in square brackets.

Table 7. Analysis of the Rydberg series converging to the 1,1-$C_2H_2Cl_2^+$ ionic. excited states $\tilde{A}^2B_2$, $\tilde{B}^2A_2$, $\tilde{C}^2A_1$ and $\tilde{D}^2B_2$. Energy positions (eV), wavenumbers (cm^{-1}), effective quantum numbers (n^*) and assignments proposed in this work are provided. Conversion factor: 1 eV = 8 065.545 cm^{-1} [11].

Energy position		Assignment
(eV)[a]	(cm^{-1})	
Converging to IE_{vert} ($\tilde{A}^2B_2$) = 11.647 eV [17]		
$4b_2 \rightarrow 3p\sigma, n^* = 2.347$		
[9.016]	72 719	$hc\omega_{av} = 34 \pm 6$ meV
[9.056]	73 041	or 274 ± 50 cm^{-1}
[9.098]	73 380	
[9.128]	73 622	
9.164	73 913	
[9.198]	74 187	EE_{vert}.
9.252	74 622	
9.278	74 832	
9.290	74 929	
$4b_2 \rightarrow 3p\pi, n^* = 2.646$		
[9.602]	77 445	$hc\omega_{av} = 25 \pm 7$ meV
[9.624]	77 623	or 200 ± 60 cm^{-1}
9.668	77 978	
[9.704]	78 264	EE_{vert}.
[9.720]	78 397	
9.742	78 742	
[9.764]	78 752	
[9.800]	79 042	
$4b_2 \rightarrow 4p\sigma, n^* = 3.417$		
10.482	84 543	EE_{vert}.
$4b_2 \rightarrow 4p\pi, n^* = 3.688$		
10.694	86 253	$hc\omega_{av} \approx 33$ meV
10.734	86 576	≈ 266 cm^{-1}
10.760	86 785	EE_{vert}.
Converging to IE_{ad} ($\tilde{B}^2A_2$) = 12.157 eV [17]		
$1a_2 \rightarrow 3p\pi, n^* = 2.46$		
9.904	79 881	EE_{ad}.
9.938	80 155	$hc\omega_{av} = 32 \pm 2$ meV
9.970	80 413	or 260 ± 8 cm^{-1}
[10.002]	80 672	
10.036	80 946	
10.064	81 171	
10.098	81 446	
$1a_2 \rightarrow 3d, n^* = 2.91$		
10.552	85 108	EE_{ad}.
10.592	85 430	$hc\omega_{av} = 36 \pm 4$ meV
10.622	85 672	or 290 ± 30 cm^{-1}
10.660	85 979	
10.694	86 253	
$1a_2 \rightarrow 4p\pi, n^* = 3.42$		
10.994	88 672	EE_{ad}.
11.018	88 866	$hc\omega_{av} = 27 \pm 3$ meV
11.048	89 108	or 218 ± 24 cm^{-1}
11.076	89 334	
11.104	89 560	
$1a_2 \rightarrow 5d, n^* = 4.92$		

Table 7. (Continued.)

Energy position		Assignment
(eV)[a]	(cm^{-1})	
11.590	93 480	EE_{ad}.
11.624	93 754	$hc\omega_{av} = 31 \pm 3$ meV
11.656	94 012	or 250 ± 24 cm^{-1}
11.684	94 238	
11.712	94 464	
	$1a_2 \rightarrow 6d, n^* = 5.97$	
11.732	94 625	n.a.
11.770	94 931	EE_{ad}.
11.807	95 189	$hc\omega_{av} = 34 \pm 4$ meV
11.838	95 480	or 274 ± 30 cm^{-1}
11.868	95 722	
	$1a_2 \rightarrow 7d, n^* = 7.04$	
11.878	95 802	EE_{ad}.
11.910	96 061	$hc\omega_{av} \approx 38$ meV
	$1a_2 \rightarrow 9d, n^* = 8.99$	
11.948	96 367	EE_{ad}.
11.984	96 657	$hc\omega_{av} = 36 \pm 3$ meV
12.020	96 948	or 290 ± 20 cm^{-1}
	Converging to IE_{ad} ($\tilde{C}^2A_1$) = 12.497 eV [17]	
	$5a_1 \rightarrow 3d, n^* = 2.89$	
10.812	87 205	
10.856	87 560	EE_{ad}.
10.892	87 850	$hc\omega_{av} = 38 \pm 10$ meV
10.914	88 027	or 300 ± 80 cm^{-1}
10.954	88 350	
	$5a_1 \rightarrow 5d, n^* = 4.94$	
11.932	96 238	EE_{ad}.
11.964	96 496	hidden in $1a_2 \rightarrow 7d$,
12.072	97 367	9d and $3b_2 \rightarrow 3d$
	$5a_1 \rightarrow 6p(\pi), n^* = 5.612$	
12.056	97 238	EE_{ad}.
12.088	97 496	$hc\omega_{av} = 33 \pm 2$ meV
12.122	97 770	or 266 ± 16 cm^{-1}
12.154	98 029	
	$5a_1 \rightarrow 8p\sigma, n^* = 7.467$	
12.244	98 755	EE_{ad}.
12.282	99 061	$hc\omega_{av} = 40 \pm 7$ meV
12.336	99 497	or 320 ± 60 cm^{-1}
12.374	99 803	
12.416	100 142	
12.456	100 464	
12.494	100 755	
12.522	101 029	
12.564	101 303	
	Converging to $IE_{ad}(\tilde{D}^2B_2) = 13.521$ eV[b] [17]	
	$3b_2 \rightarrow 3p\sigma, n^* = 2.411$	
11.182*	90 189	EE_{ad}.
11.222°	90 511	$hc\omega_A = 93 \pm 3$ meV
11.246°	90 705	or 750 ± 20 cm^{-1}

Table 7. (Continued.)

Energy position		Assignment
(eV)[a]	(cm^{-1})	
11.272*	90 898	$hc\omega_B = 32 \pm 5$ meV
11.300°	91 140	or 258 ± 40 cm^{-1}
11.332°	91 399	
11.362*	91 657	
11.398°	91 931	
11.424°	92 189	
11.458*	92 447	
11.496°	92 721	
11.524°	92 958	
11.554*	93 189	
	$3b_2 \rightarrow 3d, n^* = 2.986$	
11.996*	96 754	EE_{ad}.
12.030°	97 028	$hc\omega_A \approx 104 \pm 2$ meV
12.064°	97 303	or 839 ± 16 cm^{-1}
12.100*	97 593	$hc\omega_B \approx 34 \pm 2$ meV
12.134°	97 867	or 274 ± 16 cm^{-1}
12.168°	98 141	

[a] Energy positions corresponding to two or more assignments are given in square brackets: for explanation see text (see also tables 2 and 5).
[b] Energy positions indicated with an asterisk (*) correspond to $n\omega_A$ (n = 0–4) and with a degree symbol (°) correspond to $n\omega_B$ (n = 1–2).

Above 60 000 cm^{-1} the same authors [6] classified six sets of overlapping bands showing similar patterns and a spacing of $\omega = 1315 \pm 15$ cm^{-1}. With each member of these progressions weaker bands are observed, shifted to higher energies by about 630–700 cm^{-1} [6]. This classification and their corresponding wavenumber as reported by Walsh *et al* [6] are inserted in table 6. The assignment of the 61 209 cm^{-1} and the 60 500 cm^{-1} band is uncertain [6].

Fairly good agreement is found with the results and assignments obtained in the present work. This allows us to assign each feature in the spectrum and to remove the uncertainty concerning the 61 209 cm^{-1} and the 60 500 cm^{-1} band. A value of the wavenumbers as averaged over the six Rydberg transitions provides $\omega_3 = 1307 \pm 32$ cm^{-1} (0.162 ± 0.004 eV) and $\omega_4 = 661 \pm 40$ cm^{-1} (0.082 ± 0.005 eV). These values are very close (within the uncertainty limits) to those reported earlier [6]. Additionally, the present analysis of the 3pσ and 3pπ Rydberg transitions provides a third wavenumber $\omega_5 = 290 \pm 24$ cm^{-1} (0.037 ± 0.003 eV) assigned to the ν_5 symmetric Cl–C–Cl bending vibration [17].

Compared to [6], four additional Rydberg states converging to $IE_{ad} = 9.826$ eV are observed at higher energies, i.e., up to 10.120 eV. They also show a vibrational structure dominated by the ν_3 and ν_4 vibrational modes with an average wavenumber $\omega_3 = 1315 \pm 40$ cm^{-1} (0.163 ± 0.005 eV) and $\omega_4 = 637 \pm 40$ cm^{-1} (0.079 ± 0.005 eV). The intensity corresponding to the ν_5 vibrational mode becomes probably too weak to be observed in these members of Rydberg series characterized by higher values of the principal quantum number.

The previous discussion showed that the application of the Rydberg formula together with constant vibrational parameters throughout the series converging to a given ionic state leads to satisfactory results. This suggests that Rydberg–Rydberg and Rydberg-continuum perturbations do not affect the spectra at the spectral resolution of this study.

5.2.3. Rydberg transitions between 9.0 and 20.0 eV (see figures 1 and 2)

In this photon energy range (figures 1 and 2) several Rydberg series converge to higher lying ionization energies corresponding to the removal of an electron respectively from the $4b_2$ molecular orbital (MO) ($IE_{ad} = 11.46$ eV [19] or 11.520 eV [17]), the $1a_2$ MO ($IE_{ad} = 12.06$ eV [19] or 12.157 eV [17]), the $5a_1$ MO ($IE_{ad} = 12.497$ eV [17]), and the $3b_2$ MO ($IE_{ad} = 13.521$ eV [17]) as determined by He-I PES. In this range, the ionization of the $4a_1$ MO and $3a_1$ MO is detected at $IE_{ad} = 15.539$ eV and $IE_{ad} = 18.496$ eV respectively [17]. Several members of these Rydberg series show very strong absorption, e.g., at 9.198, 9.720 and at 10.002 eV. Above 10.4 eV the underlying photoabsorption continuum shows a continuous and steady increase. Furthermore, the PAS shows an abundant structure between 9.1 and 13.0 eV (see figure 1) whereas only broad and weak structureless bands are detected between 13 and 20 eV (figure 2).

To the best of our knowledge, no data are available in the literature on this energy range. Walsh *et al* [6] reported an 'intense, diffuse doublet' at 1350 Å (74 120 cm^{-1} or 9.190 eV) which corresponds to the absorption

maximum at 9.198 eV observed in the present work. A second band at shorter wavelength, but 'hindered by the presence of water and oxygen' is observed by Walsh *et al* [6] mentioning a maximum of absorption at 78 135 cm^{-1} (9.687 eV) which is a doublet. Also this observation should unambiguously correspond to the absorption observed at 9.720 eV in the present work. A third band is measured at 80 727 cm^{-1} (10.009 eV) in very good agreement with the energy of 10.002 eV observed in the present work. Walsh *et al* [6] interpreted these bands as members of Rydberg series converging to an ionization energy of 10.4 eV with a quantum defect $\delta = 0.66$.

Owing to the steeply increasing (and even overwhelming) intensity of the underlying continuum, the interpretation of this part of the PAS is greatly facilitated by the subtraction method (see section 2). The resulting Δ-plot in the 12–18 eV energy range is shown in figure 2. To avoid overcrowding, the result of the analysis is only partially shown by vertical bars in figure 1 between 9.0 and 13.0 eV and in figure 2 between 13 and 18 eV for the major Rydberg series. Their respective ionization limits are represented in these figures by shaded areas. The positions of the adiabatic excitation energies for the Rydberg series converging to the successive ionization limits are listed in table 2. The assignments proposed for most of these features are based on the value of their effective quantum numbers listed in the same table.

Noteworthy is that the Rydberg series observed in the 9.0–18.0 eV photon energy range are predominantly of np- or nd-character. The most intense features of the PAS involve $4b_2 \rightarrow 3p\sigma$ and $3p\pi$ and $1a_2 \rightarrow 3p\pi$ transitions (see figures 1 and 3(c)). The $1a_2 \rightarrow$ ns and $1a_2 \rightarrow np\sigma$ are symmetry-forbidden in the $C_{2\nu}$ point group. The photoelectron band corresponding to the $4b_2$ MO ionization exhibits an extended vibrational progression, involving a single vibrational mode [17]. This bell-shaped band is characterized by $IE_{ad} = 11.520$ eV and its $IE_{vert} = 11.647$ eV [17]: this latter value is used as the convergence limit for the $4b_2 \rightarrow np\sigma$ and $np\pi$ Rydberg series. The third photoelectron band (corresponding to the $\tilde{B}^2A_2$ ionic state) has $IE_{ad} = IE_{vert} = 12.157$ eV exhibiting a long vibrational progression involving Cl–C–Cl bending vibrational motion [17].

Above 13.0 eV the PAS of 1,1-$C_2H_2Cl_2$ shows a further increase of about 20% of absorption and a succession of weak broad bands (see figure 2(a)). The corresponding Δ-plot of this energy range is shown in figure 2(b). To increase the unfavorable signal/noise ratio the result is smoothed by fast Fourier transform (red curve FFTsm in figure 2(b)). Several well defined bands are clearly observed. Their respective maxima are listed in table 2. Noteworthy is the profile of the bands with maxima at 16.15 and 17.30 eV which both show a strong asymmetry on the high energy side. However, due to the low intensity and the probable superposition of vibrational transitions, we could not fit Fano profiles to these bands.

As long as the Rydberg–Rydberg and Rydberg-continua interactions might be considered as negligible, the results and assignments listed in table 2 are obtained. Two series are highlighted converging respectively to $IE_{vert} = 15.82$ eV and to $IE_{ad} = 18.496$ eV corresponding to the excited $\tilde{F}^2A_1$ and $\tilde{H}^2A_1$ states of the cation [17]. The members of both series are essentially ns/nd- and np-type Rydberg states. It will be shown that the resonant absorption of the $4a_1 \rightarrow 3p$ transition induced by the ArII resonance line at 13.48 eV provides an extended population of the $\tilde{X}^2B_1$, $\tilde{A}^2B_2$, $\tilde{B}^2A_2$ and $\tilde{C}^2A_1$ ionic states through autoionization [17]. Similarly, but to a lesser extent, the $3a_1 \rightarrow 4p$ transition induced by the NeI resonance line at 16.85 eV leads to autoionization to the same final ionic states [17].

5.2.4. Vibrational analysis (see figures 3(c) and (d))

The closeness of the first three convergence limits (IE_{ad}), i.e., 11.520, 12.157 and 12.497 eV [17], makes the vibrational analysis fairly difficult. To disentangle this part of the spectrum, the HeI-PES bands corresponding to these ionization limits have been used as a reference to perform the vibrational analysis. The sum of these overlapping contributions simulates qualitatively the Δ-plot. The resulting analysis is shown in figures 3(c), (d) and summarized in table 7.

Owing to the difficulty to determine the adiabatic excitation energy, a number of members of $np\lambda$-Rydberg series are considered to converge to 11.647 eV, i.e., the IE_{vert} of the $\tilde{A}^2B_2$ state of 1,1-$C_2H_2Cl_2^+$ [17]. The vertical excitation energies (EE_{vert}) of these members are listed in table 7. A number of the listed energy positions are in square brackets as corresponding to several possible assignments. Overlaps between close-lying transitions make the analysis difficult as shown in figure 3(c). For three Rydberg states we observe a vibrational wavenumber in the 200–270 cm^{-1} range. This value is close, though smaller, than the value measured for the $\tilde{A}^2B_2$ cation state where $\omega_5^+ = 282 \pm 40$ cm^{-1} [17] which corresponds to the Cl–C–Cl bending vibration.

From 9.9 to 10.8 eV the $1a_2 \rightarrow 3p\pi/3d$ Rydberg series show up clearly in the Δ-plot with a regular vibrational spacing (see figure 3(c)).

The Rydberg series converging to the $1a_2^{-1}$ ionization limit (the $\tilde{B}^2A_2$ ionic state) at 12.157 eV [17] all show a vibrational spacing of about 0.033 ± 0.004 meV (268 ± 32 cm^{-1}) as averaged over all observed transitions (see table 7). This energy should also correspond to the Cl–C–Cl bending vibration. This value is very close to the value measured for the $\tilde{B}^2A_2$ ionic state of 1,1-$C_2H_2Cl_2^+$, i.e., $\omega_5^+ = 266 \pm 32$ cm^{-1} [17].

To avoid overcrowding figure 3(c) and even more figure 3(d), the $5a_1^{-1}$-Rydberg vibrational transitions are not all represented but are listed in table 7. Only the vibrational progression associated with the $5a_1 \rightarrow 8p\sigma$ transition is drawn in figure 3(d). These Rydberg series are characterized by a more or less long vibrational progression with an average spacing spreading between 33 ± 2 meV (266 ± 16 cm^{-1}) and 40 ± 7 meV (320 ± 60 cm^{-1}). The most reasonable assignment corresponds to ν_5 (Cl–C–Cl symmetric bending). In the $\tilde{C}\,^2A_1$ cationic state the corresponding energy was determined at 42 ± 4 meV (339 ± 32 cm^{-1}) by HeI-PES and 39 ± 3 meV (314 ± 24 cm^{-1}) by TPES [17].

Finally Rydberg series have been observed between 11.2 and 12.17 eV with an abundant vibrational structure (see figure 3(d)). They converge to the $\tilde{D}^2B_2$ cationic state of 1,1-$C_2H_2Cl_2^+$ at IE_{ad} = 13.521 eV [17]. The $3b_2 \rightarrow 3p\sigma$ and $3b_2 \rightarrow 3d$ transitions have clearly been identified (see table 2). The associated vibrational structure with proposed assignments is listed in table 7.

For both transitions two wavenumbers are observed, i.e. ω_A = 750 ± 20 cm^{-1} and ω_B = 258 ± 40 cm^{-1} for the $3b_2 \rightarrow 3p\sigma$ transition and ω_A = 840 ± 16 cm^{-1} and ω_B = 274 ± 16 cm^{-1} for the $3b_2 \rightarrow 3d$ transition. It is noteworthy that in both cases $\omega_A \approx 3\omega_B$ within the error limits. The lowest wavenumber of 258 cm^{-1} (or 274 cm^{-1}) may likely be assigned again to the ν_5 Cl–C–Cl bending motion.

6. Conclusions

The VUV photoabsorption spectrum of 1,1-$C_2H_2Cl_2$ has been recorded at higher resolution with synchrotron radiation and thoroughly analyzed in the unexplored region above the 10.5 eV photon energy limit, up to 20 eV. Contrarily to the broad and strong bands usually observed in the high energy range, structures linked to vibrational excitation could be identified and tentatively assigned.

Quantum chemical calculations show that valence–valence ($2b_1(\pi) \rightarrow \sigma^*/3s$ and π^*) and valence-Rydberg ($2b_1(\pi) \rightarrow 3s/\sigma^*$) transitions are involved between 5 and 7.2 eV. From these calculations the σ^* and 3s states appear strongly mixed, the former being antibonding. The vibrational structure of these states has been assigned. The present data are also considered in a broader framework, by comparing them with the situation taking place in previously investigated analog molecules, that is, C_2H_4, C_2H_3Cl [1], 1,1-$C_2H_2F_2$ [3] and 1,1-C_2H_2FCl [2, 4].

Between 6.7 and 9.7 eV, many vibronic Rydberg transitions have been identified: $2b_1 \rightarrow ns$ (n = 3–7), two types of np (n = 3–13 and 3–18) and one nd (n = 3–14). These transitions involve Rydberg states converging to the 1,1-$C_2H_2Cl_2^+(\tilde{X}^2B_1)$ ground ionic state. The vibrational structure associated with these transitions has been analyzed based on the data for the first band of the 1,1-$C_2H_2Cl_2$ HeI-PES [17]. The harmonics and combination transitions involving three vibrational modes, that is, ν_3 = 1307 cm^{-1} (C=C stretching), ν_4 = 661 cm^{-1} (C–Cl symmetric stretching) and ν_5 = 290 cm^{-1} (Cl–C–Cl bending), have been identified.

Above 9.0 eV and up to 12.6 eV numerous transitions to Rydberg states converging to the successive excited states of 1,1-$C_2H_2Cl_2^+$ are observed. For most of them vibrational progressions are observed. Assignments are proposed and nearly all vibrational structures may be accounted for by the excitation of the Cl–C–Cl bending vibration with a wavenumber in the 210–290 cm^{-1} range.

Between 12.6 and 18.5 eV weak broad bands are superimposed on a strong continuum. Several Rydberg transitions are observed converging to the $4a_1^{-1}$ and $3a_1^{-1}$ ionization limits.

Acknowledgments

We acknowledge the financial contribution of the University of Liège and the support of the European Community to access the BESSY large-scale synchrotron facility. DD's contribution was supported by the Belgian program on Interuniversity Attraction Poles of the Belgian Science Policy (IAP n° P6/19).

ORCID iDs

R Locht https://orcid.org/0000-0002-9175-2720

References

[1] Locht R, Leyh B, Dehareng D, Jochims H-W and Baumgärtel H 2009 *Chem. Phys.* **362** 97
Locht R, Leyh B, Hottmann K and Baumgärtel H 1997 *Chem. Phys.* **220** 207
Hoxha A, Locht R, Leyh B, Dehareng D, Hottmann K, Jochims H-W and Baumgärtel H 2000 *Chem. Phys.* **260** 237
[2] Tornow G, Locht R, Kaufel R, Baumgärtel H and Jochims H-W 1990 *Chem. Phys.* **146** 115
[3] Locht R, Jochims H-W and Leyh B 2012 *Chem. Phys.* **405** 124
Locht R, Dehareng D and Leyh B 2012 *J. Phys. B: At. Mol. Opt. Phys.* **45** 115101
[4] Locht R, Dehareng D and Leyh B 2014 *Mol. Phys.* **112** 1520

[5] Teegan J P and Walsh A D 1951 *Trans. Faraday Soc.* **47** 1
[6] Walsh A D, Warsop P A and Whiteside J A B 1968 *Trans. Faraday Soc.* **64** 1432
[7] Berry M J 1974 *J. Chem. Phys.* **61** 3114
[8] Marmet P 1979 *Rev. Sci. Instrum.* **50** 79
Carbonneau R, Bolduc E and Marmet P 1973 *Can. J. Phys.* **51** 505
[9] Carbonneau R and Marmet P 1973 *Can. J. Phys.* **51** 2203
Carbonneau R and Marmet P 1974 *Phys. Rev.* A **9** 1898
[10] Palmer M H *et al* 2016 *J. Chem. Phys.* **144** 204305
Palmer M H *et al* 2016 *J. Chem. Phys.* **144** 124302
Palmer M H *et al* 2015 *J. Chem. Phys.* **143** 164303
[11] Mohr P J, Taylor B N and Newell D B 2016 *J. Phys. Chem. Ref. Data* **45** 043102
Mohr P J, Newell D B and Taylor B N 2016 *Rev. Mod. Phys.* **88** 035009
[12] Frisch M J *et al* 2009 *Gaussian 09* Revision A.02 (Wallingford CT: Gaussian Inc.)
[13] Dunning T H Jr 1989 *J. Chem. Phys.* **90** 1007
[14] Zhao Y and Truhlar D G 2008 *Theor. Chem. Acc.* **120** 215
[15] Van Caillie C and Amos R D 2000 *Chem. Phys. Lett.* **317** 159
[16] Ashfold M N R, King G A, Murdock D, Nix M G D, Oliver T A A and Sage A G 2010 *Phys. Chem. Chem. Phys.* **12** 1218
[17] Locht R, Dehareng D and Leyh B *J. Phys. Commun.* at press (https://doi.org/10.1088/2399-6528/aa9129)
[18] Jonathan N, Ross K and Tomlinson V 1970 *Intern. J. Mass Spectrom. Ion Phys.* **4** 51
[19] Lake R F and Thompson H 1970 *Proc. R. Soc. London* **A315** 323
[20] Wittel K and Bock H 1974 *Chem. Ber.* **107** 317
[21] Von Niessen W, Åsbrink L and Bieri G 1982 *J. Electr. Spectry. Rel. Phenom.* **26** 173
[22] Robin M B 1985 *Higher Excited States of Polyatomic Molecules* vol 3 (Orlando: Academic) p 239
Robin M B 1975 *Higher Excited States of Polyatomic Molecules* vol 2 (New York: Academic) p 56
[23] S. Arulmozhiraja S, M. Ehara M and H. Nakatsuji H 2008 *J. Chem. Phys.* **129** 174506
[24] Chandra M, Senapati D, Tak M and Das P K 2006 *Chem. Phys. Lett.* **430** 32
[25] Hua L, Zhang X, Lee W-B, Chao M-H, Zang B and Lin K C 2010 *J. Phys. Chem.* A **14** 37
[26] Khvostenko O G 2014 *J. Electr. Spectr. Rel. Phenom.* **195** 220
[27] Shimanoushi T 1972 *Tables of Molecular Vibrational Frequencies* (*NSRDS-NBS 39*) Consolidated vol 1 (Washington DC: US Gov. Print. Off.)
[28] Locht R *et al* 2009 *Chem. Phys.* **365** 109